Cell Reports, Volume *36*

Supplemental information

Reshaping of the androgen-driven chromatin landscape in normal prostate cells by early cancer drivers and effect on therapeutic sensitivity

Ivana Grbesa, Michael A. Augello, Deli Liu, Dylan R. McNally, Christopher D. Gaffney, Dennis Huang, Kevin Lin, Daria Ivenitsky, Ramy Goueli, Brian D. Robinson, Francesca Khani, Lesa D. Deonarine, Mirjam Blattner, Olivier Elemento, Elai Davicioni, Andrea Sboner, and Christopher E. Barbieri

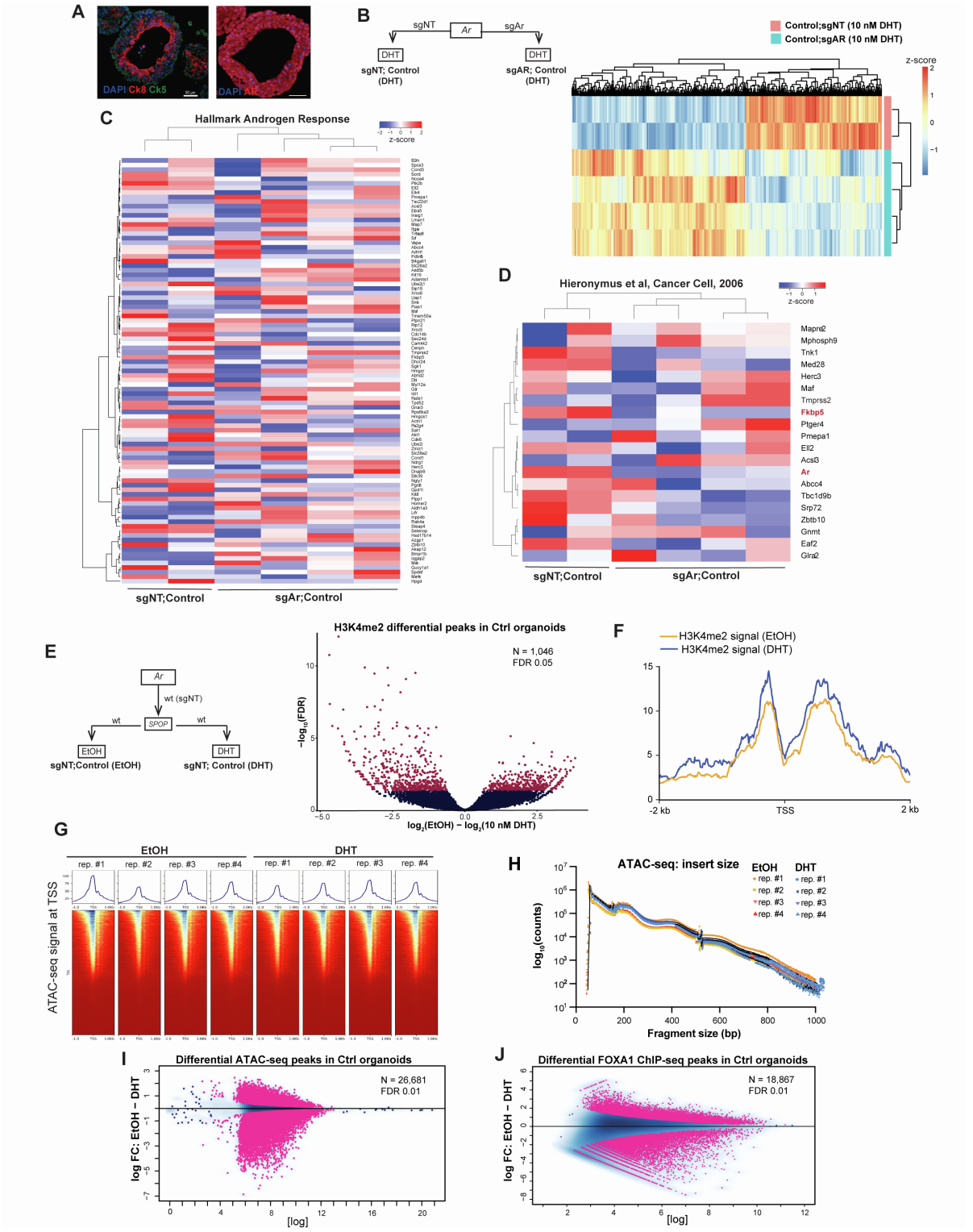

Fig. S1. Distinct changes in androgen-induced chromatin and transcriptional landscape of normal murine prostate cells (wild-type SPOP), related to Figure 1. **(A)** Morphology of murine prostate organoids (left: IF for Ck5 and Ck8) expressing AR (right). **(B)** Schematic representation of RNA-seq experiment and the heatmap showing all the differentially

expressed genes. **(C-D)** Response of human AR-target genes, from GSEA **(C)**, and literature (Hieronymus et al., 2006) **(C)**, to Ar downregulation in normal murine prostate organoids. **(E)** Schematics of the ChIP-seq and ATAC-seq experiments (left). Right – Volcano plot showing dynamics H3K4me2 ChIP-seq peaks at FDR 0.05. **(F)** H3K4me2 signal at the promotors of the AR-upregulated genes in Control organoids (shown in Figure 1c). **(G)** ATAC-seq quality metrics - distribution of DNA fragments in generated ATAC-seq libraries. **(H)** ATAC-seq quality metrics – enrichment of ATAC-seq signal at the transcription starts sites (TSS) of housekeeping genes. **(I)** Dynamic ATAC-seq peaks at FDR 0.01. **(J)** Dynamic FOXA1 ChIP-seq peaks at FDR 0.01.

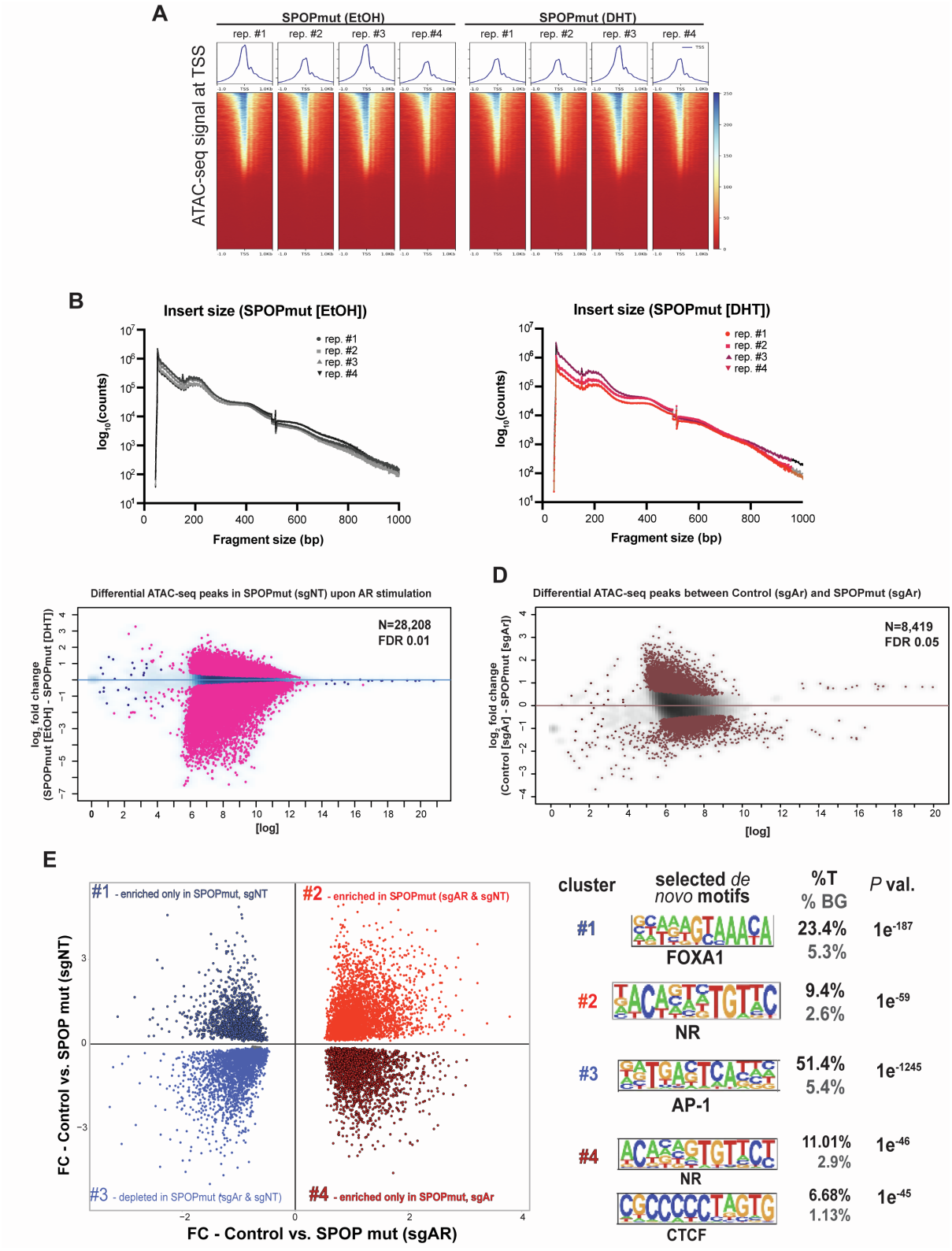

Fig. S2. Androgen-dependent and independent chromatin remodeling of murine prostate cells upon introduction of *SPOP* mutation, related to Figure 2. **(A-B)** Results of Encode quality metrics for ATAC-seq on *SPOP* mutant cells (sgNT) before and after DHT treatment -

enrichment at the promoters (i.e. TSS) **(A)** and fragment size distribution **(B)**. **(B)** MA plot – dynamic accessible region upon AR activation. **(D)** MA plot – dynamic regulatory regions induced by *SPOP* mutation when Ar is downregulated. **(E)** Scatter plot – common and unique accessible regions in SPOP mutant cells upon lower Ar expression. Right: results of de novo motif analysis. Black - target regions (%T). Grey - background regions (%BG).

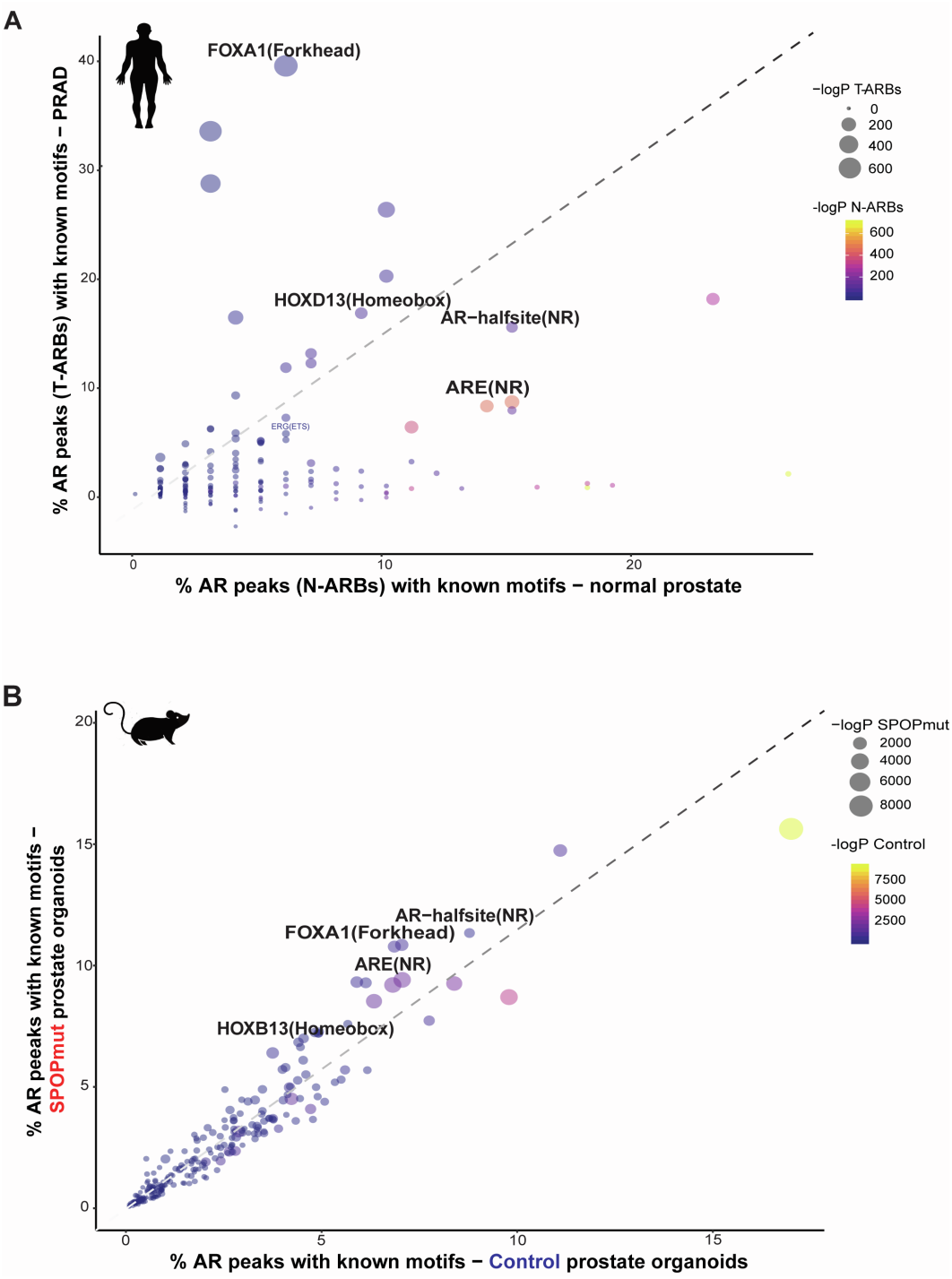

Fig. S3. AR cistrome from *SPOP* mutant cells is enriched for FOXA1 and HOXB13 motifs, related to Figure 3. **(A)** Comparison of the motifs found in AR peaks in normal human prostate tissues and cancers (Pomerantz et al., 2015). **(B)** Motifs found in AR bound regions in before and after introduction of SPOP mutation in normal murine prostate cells.

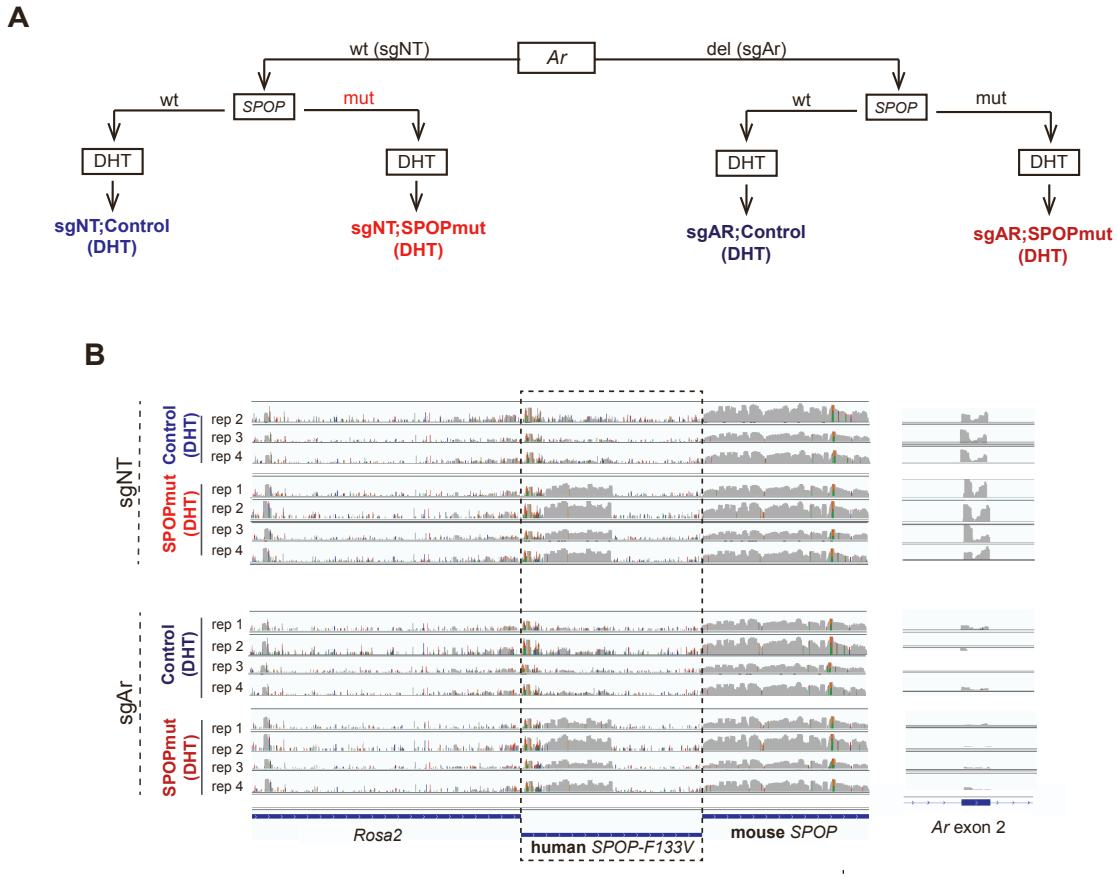

Fig. S4. RNA-seq quality control, related to Figure 5A. **(A)** Schematic representation of all the generated RNA-seq libraries. **(B)** Quality controls of the data – reads were aligned to human SPOP sequence (left) and the Ar exon 2 (sgAr target).

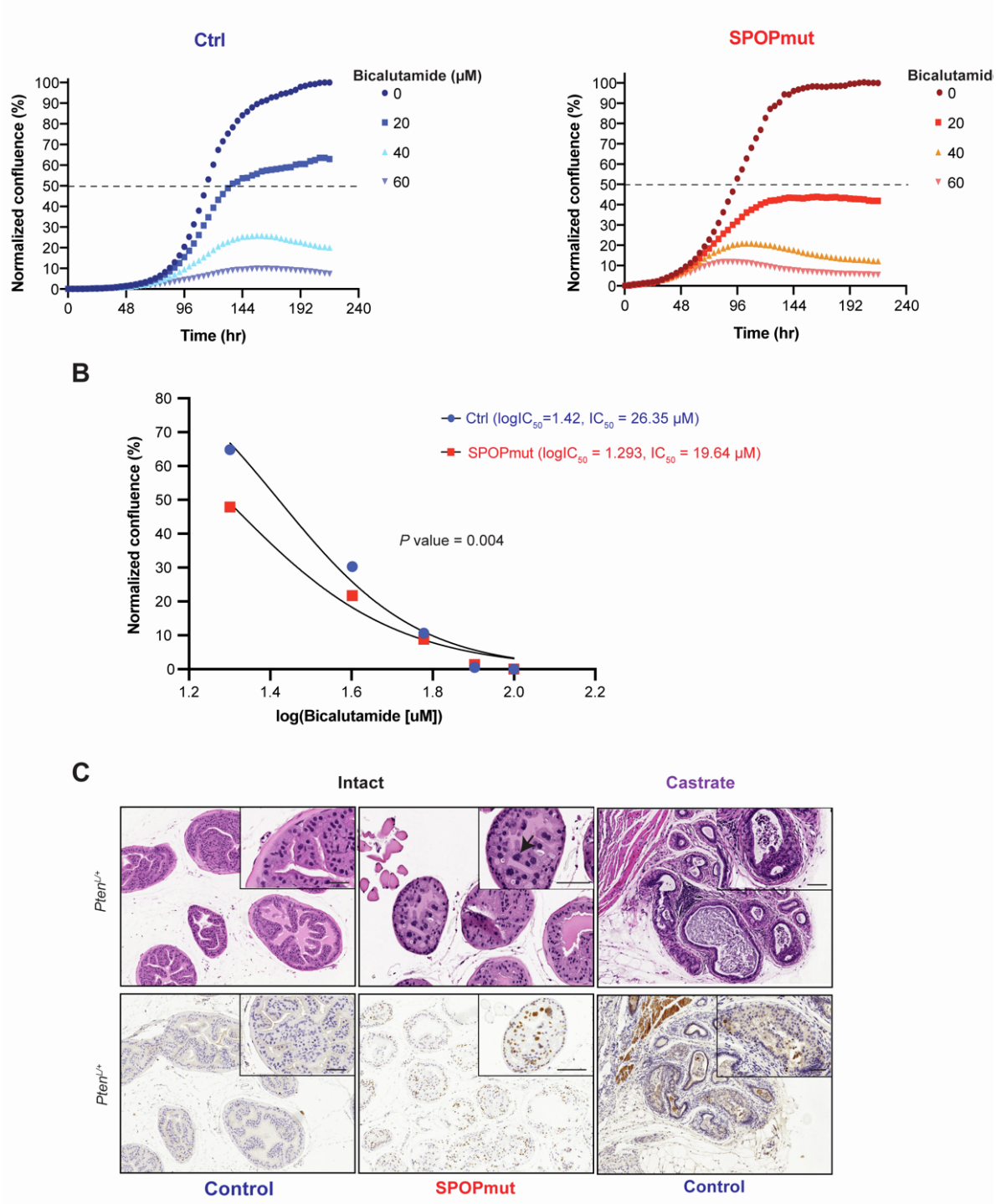

Fig. S5. Murine SPOPmut prostate cells show higher sensitivity to anti-androgen treatment, related to Figure 6. **(A-B)** Slower proliferation of *SPOP*-mutant cells when treated with bicalutamide in 2D (**A**) and 3D (**B**). **(C-D)** Representative images showing nuclear atypia and H&E staining. Scale bar, 50 μm.

Table S3. Patient's characteristics from Decipher retrospective cohort used for analysis in Fig. 7A.

	***SPOP* mutant**	***SPOP* wild-type**
Cases	168	1,458
Median age (range)	65 (44-77)	62 (37-83)
Median PSA (range)	8.9 (1.9-87)	8.6 (0.1-201)
Gleason score (range)		
<=6	16	176
3+4	30	381
4+3	24	175
>=8	60	589
Pathological tumor stage		
pT2	66	464
pT3/4	82	722
Extracapsular extension	88 (53%)	855 (61%)
Lymp node invasion	20 (12%)	228 (16%)
Seminal vesicle invasion	35 (21%)	452 (32%)
Surgical margin	68 (41%)	703 (49%)